Decoration of Titania Nanofibres with Anatase Nano-paticles as Efficient Photocatalysts for Decomposing Pesticides and Phenols

*Blain Paul, Ashley Locke, Wayde N. Martens, Ray L. Frost**

Discipline of Chemistry, Queensland University of Technology, Brisbane, Qld 4001, Australia,

Email*: r.frost@qut.edu.au, Fax: +61 7 3138 1804

Abstract

Using a series of partial phase transitions, an effective photocatalyst with fibril morphology was prepared. The catalytic activities of these materials were tested against phenol and herbicide in water. Both H-titanate and TiO_2-(B) fibres decorated with anatase nanocrystals were studied. It was found that anatase dotted TiO_2-(B) fibres prepared by a 45 h hydrothermal treatment followed by calcination were not only superior photocatalysts but could also be readily separated from the slurry after photocatalytic reactions due to its fibril morphology.

Keywords:

Photocatalytic activity
Mixed-phase titania nanofibres
Decomposition of pesticides and phenols
Removal of pesticides from the environment

1. Introduction

Extensive research is currently underway to develop low dimensional semiconductor photocatalysts for the environmental remediation of water and air. Various photocatalysts have been used successfully to degrade a wide variety of compounds [1-4]. Among the various oxide semiconductor photocatalysts that many be used, TiO_2 is one of the primary photocatalyst due to it durability, nontoxic and highly active nature. The anatase form of TiO_2 is the most photoactive and therefore is most suitable for environmental applications [5-10]. The rutile form is much less active towards most photocatalytic reactions [11-16]. Tanaka et al. have presented the photocatalytic decomposition of a wide range of compounds over different TiO_2 polymorphs and have also presented the effect of calcination temperature on the TiO_2 prepared from different methods [17]. Martin et al. showed that the rate of photo-degradation of 4-chlorophenol over anatase increased as the calcination temperature increased from 100 to 400 ^oC but decreased when the titania was heated above 500 ^oC [18].

It is almost impossible to predict the rate and extent of the photocatalytic decomposition of a compound only by using the porosity, surface area, nanoscale size or morphology of the aggregates. This is due to the non-linear correlation between structural characteristics and photocatalytic activity. Photocatalysts with morphologies such as wires, rods, tubes and fibres have been both supplementary and complementary to some of the more conventional materials for the decontamination of hazardous chemical wastes since the pioneering work of Kasuga et al. [19-26]. By optimising the preparation conditions, high-yield semiconductor photocatalyst with varied nanostructures have been prepared [27-29]. Hydrogen titanate can be used to design various TiO_2-related materials through hydrothermal treatment followed by well controlled calcination [25, 30-32]. Most procedures for the modification of structure and morphology of these titanate materials belong to the thermal evolution of Na-free titanate structures. Many different thermal conditions have been studied in order to evaluate their effect on the final product morphology. Recent thermal studies of sodium-free titanate ($H_2Ti_3O_7$) nanofibres have suggested that by heating to between 300 to 500 ^oC, the nanofibres were transformed into TiO_2-(B) while still maintaining the fibrous morphology [25, 33]. These TiO_2-(B) nanofibres could then further transform into an anatase structure by calcining them at 700 ^oC, while still retaining the fibrous shape. Only once the temperature was raised above 1000 ^oC were the nanofibres

transformed into rode-shaped rutile [25, 33]. It is well documented in the literature that the photocatalytic activity of a titania can be improved by using a binary phase system, which is a catalyst composed of two crystal forms of TiO_2 with a small differences in band gaps.

Improved photocatalytic activity, over that of P25, for the production of hydrogen from ethanol was observed for a mixed-phase nanocomposite which consisted of 33% TiO_2-(B) nanotubes and 67% anatase nanoparticles, which were prepared from H-titanate nanotubes [34]. Further to this, anatase particles have also been coated onto the surface of titanate nanotubes and nanofibres by the hydrolysis of TiF_4 in the presence of H_3BO_4 [34-35]. When trying to explanation the photocatalytic activities of titanate nanowires and nanotubes, it is important to compare them with the source material and to clarify the effect of phase structure, crystallite size, electronic and morphological changes. The following investigation will investigate the photocatalytic activities of H-titanate and TiO_2-(B) nanofibres, which have been decorated with anatase nanoparticles. The direct electrical contact between the anatase nanoparticles and the fibres themselves is expected to provide an efficient charge-transfer region, which would make this binary system suitable for photocatalysis.

2. Experimental Section

2.1 Materials and Sample preparation

The TiO_2 source used for the preparation of the titanate was commercial grade TiO_2 powder (P25, Degussa AG) which is a mixture of 20% rutile and 80% anatase with particle size of around 30 nm. In a typical synthesis, 6 g of TiO_2 powder was mixed with 80 mL of 10 M NaOH solution [26, 31-32]. The suspensions were agitated in an ultrasonic bath for 30 min which was followed by hydrothermal treatment of the mixture in a Teflon-lined stainless steel autoclave at 180 ^oC for 48 h. After the hydrothermal treatment, the precipitate (sodium titanate nanofibres) were separated by filtration and washed with distilled water to remove excess NaOH. The washed precipitate was then exchanged with H^+ by washing with a 0.1 M HCl solution to produce $H_2Ti_3O_7$ nanofibres, and washed again with distilled water until the pH value of the rinsing solution reached ~ 7. The washed samples were dried at 80 ^oC for 12 h. The mixed phase photocatalysts were prepared by successive modification of $H_2Ti_3O_7$ nanofibres. The coating of anatase nanoparticles on the surface of $H_2Ti_3O_7$ nanofibres were carried out in a hydrothermal process [36]. In a typical procedure, 0.4 g of $H_2Ti_3O_7$ nanofibres and 40 mL of 0.05 M HNO_3

acid solution were put into a Teflon-lined stainless autoclave. The autoclave was heated at 110 ^{o}C for 15, 30, 40, 45 h and 5 days, respectively. The amount of coating was substantially controlled by the duration of the hydrothermal treatment. The TiO_2-(B) photocatalysts with anatase particles on the surface were prepared by using the following procedure. The $H_2Ti_3O_7$ nanofibres dotted with anatase nanocrystals were calcined at 450 ^{o}C to convert the $H_2Ti_3O_7$ into the TiO_2-(B). It is noteworthy that the anatase crystals on the surface remain unchanged during the heating process. After calcination TiO_2-(B) fibres with varying amounts of anatase crystals on the surface were obtained. HA1, HA2, HA3, HA4 and HA5 represent titanate fibres with anatase shells based on the increasing order of the hydrothermal treatment time. For comparison, pure $H_2Ti_3O_7$ fibres labelled as 'H' and pure TiO_2-(B) fibres as 'T' were synthesized by heating the $H_2Ti_3O_7$ nanofibres at 723 K. For instance, HA1 is the sample obtained after 15 h of hydrothermal treatments. CA1, CA2, CA3, CA4 and CA5 represent the TiO_2-(B) core with the anatase shell.

2.2. Characterisation

Surface analysis based upon the N_2 adsorption/desorption technique was conducted on a micrometrics Tristar 3000 automated gas adsorption analyzer after sample pretreatment at 110 ^{o}C for 12 h under a flow of N_2. XRD patterns were recorded between 5 and 90 ^{o} (2θ) using Cu Kα radiation (λ= 0.15418 nm) on a Philips PANalytical X' pert PRO diffractometer operation at 40 kV and 40 mA with a 0.25 ^{o} divergence slit and a 0.5 ^{o} antiscatter slit. TEM images of samples were obtained with a Philips CM 200 transmission electron microscope operating at 200 kV. All Samples were recorded on a Cary 100 spectrometer with a scan range of 200 to 900 nm. Raman spectra were collected by a Renishaw Ramascope spectrometer equipped with a He-Ne laser (633 nm). The spectrometer was operated at a resolution of 2 cm^{-1} in the range between 100 and 1600cm^{-1}. Repeated acquisitions using the highest magnification were accumulated to improve the signal-to-noise ratio in the spectra. Spectra were calibrated using the 520.5 cm^{-1} line of a silicon wafer.

2.3. Photocatalytic Activity

Illumination of sample slurries were carried out by using UV light source with six tubular 38W Hg lamp (NEC, FL20BL T8), with a peak wavelength at about 365 nm. The catalyst concentration was 50 mg per 50 ml with the initial concentration (C_0) of phenol is being 25 ppm.

The initial concentration of simazine was 5 ppm each, due to the reduced solubility of these compounds. The catalyst powder and herbicide solution were mixed in the dark for 30 min in Pyrex glass vessels to ensure surface equilibration prior to irradiation. These reactors were placed on a magnetic stirring plate with the suspension surface at a fixed distance of 25 cm from the lamps. This UV light source was attached vertically to the internal top of a wood box (100cm × 35cm × 35cm). One fan was positioned in order to minimize the heat effect generated by the lamp. During the reaction, the liquid of the reaction system was collected every 15 min, and the samples filtered through a 0.45 μm Millipore filer prior to the analysis. The filtrates of phenol and simazine were analyzed by using a Cary 100 UV spectrophotometer, at absorbance 270 and 222 nm.

3. Results and discussion

3.1. XRD patterns

The mixed phases fibre photocatalysts were examined by powder XRD (Fig 1). A corresponding XRD patterns (Fig 1a) exhibited obvious diffraction peaks of anatase in addition to the sharp peaks of trititanate, suggesting that nanocrystals coated on the surface of the titanate nanofibres were anatase. The pure hydrogen titanate nanostructures have peaks at 2θ values of 9.6^{o}, 24.7^{o}, 28.02^{o}, 48.22^{o} and 62^{o}, which can be attributed to the 020, 110, 130, 200, and 002 peaks respectively [37-38]. It is clear that samples HA1, HA2, HA3, and HA4 contained mixed phases of hydrogen titanate and anatase which are indicated in Figure 1a. The peak intensity corresponding to the anatase increases from HA1 to HA4, whereas in HA5, the hydrogen titanate disappeared, completely converting to anatase after the 5 days of hydrothermal treatment. As can be seen in the Figure 1b, upon calcination at 450 ^{o}C the characteristic peaks of titanate have disappeared and new peaks of TiO_2-(B) appeared. As the calcination proceeds, the width of the anatase peaks slightly increased due to improved crystallinity while the hydrogen titanate phase is converted into metastable TiO_2-(B). The diffraction peaks of samples CA1, CA2, CA3, and CA4 in Figure 1b could be indexed to the anatase and TiO_2-(B) phases. The average crystallite size of all the samples calculated using the Scherrer equation is presented in Table 1. With an increase in hydrothermal treatment time from 15 h to 4 days, the crystallite size of the anatase increased from 10.16 to 16.15 nm. Calcination to 450 °C also increased the crystallites size of anatase, with crystallite sizes reaching 17.9 nm.

3.2. Raman spectroscopy

Phase transformation of mixed phase fibre photocatalysts can be confirmed by the analysis of their Raman spectra. Figure 2 displays the spectra of hydrogen titanate consisting of very broad bands near 195, 280, 450 and 680 cm^{-1} respectively. The peaks observed at 145, 197, 399, 518 and 640 cm^{-1} can be assigned as the E_g, B_{1g}, A_{1g} or B_{1g} and E_g modes of the anatase phase [39]. The lowest frequency E_g mode at 145 cm^{-1}, indicates the existence of the long-range order of the anatase phase, whereas the weak broader peaks in the high-frequency region indicate the lack of short range order in the anatase phase [40]. High frequency Raman bands of HA5 and CA5 indicated that samples were highly pure with few defects and were likely to be pure anatase in phase. The position, relative intensity and width of the lowest-frequency E_g mode is known to be closely related to the particle size of the anatase phase [41]. As the hydrothermal treatment time increases, the intensity of the lowest frequency E_g mode increases. These observations demonstrate the hydrothermal-dependent evolution of the anatase phase. The spectrum observed for sample CA1 (Figure 2b) shows very similar peak positions and profiles to that of bulk TiO_2-(B) [42]. It is evident that, the abundance of sharp peaks gradually decreases in intensity as the amount of TiO_2-(B) phase decreases. These become completely absent in the spectrum of CA5.

3.3. TEM and SEM images

The morphology and microstructural details of the anatase particles coated on the surface of H-titanate and TiO_2-(B) fibres are shown in Figures 3 and 4 respectively. TEM images clearly display the discrepancies between the surfaces of pure and anatase dotted fibres. Figure 3b-e confirmed that a large number of isolated anatase particles were formed and are randomly oriented in the surface of fibres. Based on the visual information obtained from TEM, it can be confirmed the existence of randomly dispersed antase particles which inturn enhance the light trapping ability of the catalyst. SEM micrographs (Figure 3) show the different degrees of morphological change experienced after the hydrothermal treatment for the coating of the anatase particles on the surface of H-titanate nanofibres. We can observe in Figure 4a that the H-titanate fibres are smooth with a length larger than several micrometers. With prolonged hydrothermal treatment there is slightly destruction of the fibrous morphology and changed more into particle, as seen in Figure 4d and 4d1. It was noted in the photocatalytic studies that these

more particulate type morphologies have a strong tendency to agglomerate and are difficult to be separated out completely from a slurry system after the photocatalytic reaction.

3.4. UV-visible Spectroscopy

UV-visible spectra of mixed phase fibre photocatalysts are shown in Figure 5. All the tested samples exhibited an absorption band in the UV region. The adsorption edge of all calcined samples (Figure 5b) shifted to the blue regime. The band gap (energy gap, E_g) can be calculated for practical purposes by using Equation (1) [43]. The absorbance wavelength (λ) can be obtained by extrapolating the linear part of the corresponding curves to the abscissa axis.

$$E_g = 12400/\lambda \quad (1)$$

where λ is the absorbance wavelength.

Anatase nanoparticles dispersed on a large-bandgap matrix are expected to be different to those of the bulk materials. The slight blue shift in the absorption edge after calcination is probably due to an increase in crystallinity, a decrease in the concentration of the defects in the structure and the removal of the volatile impurities [44].

3.5. Surface Area

The N_2 sorption isotherms for the mixed phase fibre catalysts are presented in Figure 6. It was noted that all samples have very low surface areas. It can be seen that all of the isotherms are typically of a type H3 hysteresis loop according to the BDDT classification system [45]. However, an almost negligible amount of hysteresis was observed in all of the tested samples, indicating only a small amount of or the complete absence of mesopores (2-50 nm). A large nitrogen uptake is observed close to the saturation pressure, where the capillary condensation of the aggregates of titanate nanofibres starts. Moreover, in all of the tested samples the hysteresis loops approach $P/P_0 = 1$, suggesting the presence of macropores (>50 nm) [46]. On the other hand, the areas of the hysteresis loops gradually increase upon increasing the hydrothermal treatment time. A remarkably small adsorption at low P/P_0 was noted for all the samples, which indicates a very low microporosity. A steep increase in P/P_0 position for the samples with long hours of hydrothermal treatment was observed, which indicated changes in the texture of the crystals after the prolonged treatment [36].

The isotherms shown in Figure 6 suggest that the pore volume increases as the content of anatase nanoparticles increase from H1 to H5 depending on the hydrothermal treatment time. As seen in Table 1, there was also a significant increase for S_{BET} from 28.4 to 64 m^2/g and an increase in pore volume from 0.08 to 0.33 cm^3/g, along with the formation of the anatase nanoparticles on the surface of H-titanate nanofibres. Sample HA5 shows a slight decrease in surface area. This can be attributed to the complete phase transition from H-titanate to anatase, which results in changes in the fibrillar morphology. It is worth noting that the average pore diameter increases after calcination at 450 ^oC. This might be caused by the decrease in the wall thickness of the anatase crystals.

3.6. Photocatalytic activity

Figures 7 to 8 show the degradation profile of phenol and simazine respectively. No detectable amount of degradation was observed in the absence of the catalysts. The photocatalytic activities of the H-titanate and TiO_2-(B) fibres before and after the coating of the anatase nanoparticles were evaluated. It was found that without the coating of the anatase particles both titanate and TiO_2-(B) fibres has little photocatalytic activity. After the anatase nanoparticles were uniformly coated on the surface of the nanofibres, the samples showed a high photocatalytic activity, which was dependent on the amount of deposition on the surface. Notably, the role of adsorption was less important, while the treatment time for degradation was more important. It was found that as synthesized TiO_2-(B) fibres showed greater, although still small, photocatalytic activity compare to the H-titanate fibres. The complete removal of phenol was observed to occur in the presence of HA5, CA3 and CA4 after 120 min of UV illumination. However, in the case of HA5, the fibre morphology is almost diminished whereas CA3 and CA4 still have fibre morphology. Phenol is considered as one of the most difficult organic pollutants to degrade, so it is easy to guess that degradation rates of other phenolic complounds which would be much higher than the degradation rates of phenol. The data indicates that simazine is also one of the most difficult herbicides to degrade (Figure 8). Only a small decrease in the concentration of phenol was detected with catalysts H and T. An almost identical pattern of degradation was observed for both pollutants except for the overall degradation rate. Therefore it is reasonable to summarise that anatase decorated TiO_2-(B) fibres are one of the most active novel photocatalysts for the application of pollutant degradation in water. As stated previously, the crystal size is an important parameter for achieving superior activity in a photocatalyst. The higher photocatalytic

may not be related with the surface area. The crystal size calculated for anatase particles for HA5 and CA4 are 16.1 and 16.9 nm (Table 1), respectively.

3.7. Mechanism

The high photocatalytic activities of CA3 and CA4 (TiO_2-B core with anatase particles on the surface) can be explained by considering two factors. One is the light trapping ability of the surface layer anatase and other is the depth of the interaction of two different phases which are in physical contact each other [47-48]. The performance of pure anatase phase as a photocatalyst is related to the charge-carrier dynamics and the degradation of various pollutants, which proceed through a complicated multistep interfacial charge transfer process. The efficiency of the catalyst depends on the rate of recombination of electron and hole pairs and also the charge transfer across the solid-liquid interface. The charge carriers either recombine within the bulk of the material or move to the surface of the particle where they can also recombine or can be trapped at defect sites. The holes can react with surface hydroxyl groups which produce strong oxidising hydroxyl radicals, which again react with the organic compounds leading to complete mineralisation. The electrons interact with molecular oxygen to form the superoxide radical anion, $O_2^{\bullet-}$ [9]. If the rate of recombination of electrons and holes increases, then the efficiency of the interfacial charge transfer decreases which leads to a decrease in the speed of photo reactions. The efficiency of a catalyst depends on the ability to slow down the recombination of electrons and holes. The recombination rate is dependent on the defects in the samples and may be due to the different sample preparation conditions that lead to materials with a particular morphology and various different crystal defects.

As seen in Figure 9, the chemical potential of electrons in the semiconductor represented by the position of the Fermi level and the chemical potential of the solution depends on the dissolved substance in the solution. Semiconductors always experience a flow of electrons when it contacts with an electrolyte and vice versa. This flow is dependent on the chemical potentials of the electrolyte and the photocatalysts. Interestingly, in the case of the anatase photocatalyst (n-type) the excess electrons move to the electrolyte and leave a positive charge in the semiconductor and negative charge in the electrolyte. These charge separations are located at the solid-liquid interface and the established Schottky barrier [49]. The electric field formed in the Schottky barrier causes the bending of VB and CB at the solid–liquid interface. Because of the charge

separation in the solid–liquid interface, holes in the valence band formed after the migration of electrons to the conduction band diffuse to the surface. At the same time, electrons in the conduction band move in the opposite direction, due to the lower energy of CB in the TiO_2-(B)solid. These electrons can again migrate into the lowest energy of the conduction band in the TiO_2-(B) phase induced by the space-charge layers [47]. This kind of inter-band migration suppresses the electron-hole pair recombination. This assures the electron-hole pair a lifetime which is sufficiently long to enable these species to participate in interfacial electron transfer.

4. Conclusions

It has been seen that the photocatalytic activities of anatase decorated titanate as well as the TiO_2-(B) fibres prepared in a series of phase transition processes were superior in performance as a photocatalysts. The intimate contact between the two phases inhibits the recombination of excited state conduction band electrons and valence band holes by the possible migration of electrons into the lower energy conduction band of the TiO_2-(B) fibril core. The multiphase structures achieved a phase charge layer between the two phases facilitating the passage of charges with each other. These novel multiphase photocatalysts have the potential to alleviate the disadvantages associated with powdered photocatalysts as well as thin film photocatalysts. Moreover, the obtained anatase decorated TiO_2-(B) fibres prepared by a 45 h hydrothermal treatment followed by calcination is not only superior in performance as photocatalysts but they could also be readily separated out from the slurry system after photocatalytic reactions.

Acknowledgements

This work was supported by ARC. The author is grateful to Prof. H.Y. Zhu and Dr. Dongjiang Yang for their aid in the data analysis.

References

[1] S.O. Pehkonen, R. Siefert, Y. Erel, S. Webb, M.R. Hoffmann, Environ. Sci.Technol. 27 (1993) 2056-2062.
[2] D.W. Bahnemann, C. Kormann, M.R. Hoffmann, J. phys. Chem. 91 (2002) 3789-3798.
[3] D.W. Bahnemann, C. Kormann, M.R. Hoffmann, J. Phys. Chem. 91 (1987) 3789-3798.
[4] A.J. Hoffman, E.R. Carraway, M.R. Hoffmann, Environ. Sci. Technol. 28 (2002) 776-785.
[5] S. Nishimoto, B. Ohtani, H. Kajiwara, T. Kagiya, J. Chem. Soc. Faraday Trans. 1 81 (1985) 61.
[6] E.R. Carraway, A.J. Hoffman, M.R. Hoffmann, Environ. Sci. Technol. 28 (2002) 786-793.
[7] H. Hidaka, J. Zhao, E. Pelizzetti, N. Serpone, J. Phys. Chem. 96 (2002) 2226-2230.
[8] G. Mills, M.R. Hoffmann, Environ. Sci. Technol. 27 (2002) 1681-1689.
[9] E. Pelizzetti, C. Minero, P. Piccinini, M. Vincenti, Coord. Chem. Rev. 125 (1993) 183-193.
[10] M.V. Rao, K. Rajeshwar, V.R.P. Verneker, J. DuBow, J. Phys. Chem. 84 (2002) 1987-1991.
[11] A. Mills, S. Morris, R. Davies, J. Photochem. Photobiol. A: Chem. 70 (1993) 183-191.
[12] B.V. Mihaylov, J.L. Hendrix, J.H. Nelson, J. Photochem. Photobiol. A: Chem. 72 (1993) 173-177.
[13] S.T. Martin, C.L. Morrison, M.R. Hoffmann, J. Phys. Chem. 98 (2002) 13695-13704.
[14] A. Mills, R.H. Davies, D. Worsley, Chem. Soc. Rev. 22 (1993) 417-425.
[15] K.E. Karakitsou, X.E. Verykios, J. phys. Chem. 97 (2002) 1184-1189.
[16] H. Noda, K. Oikawa, H. Ohyanishiguchi, H. Kamada, Bull. Chem. Soc. Jpn. 66 (1993) 3542-3547.
[17] K. Tanaka, T. Hisanaga, A.P. Rivera, In Photocatalytic Purification and Treatment of Water and Air, Elsevier, Amsterdam, 1993.
[18] S.T. Martin, C.L. Morrison, M.R. Hoffmann, J. phys. Chem. 98 (1994) 13695-13704.
[19] T. Kasuga, M. Hiramatsu, A. Hoson, T. Sekino, K. Niihara, Adv. Mater. 11 (1999) 1307.
[20] T. Kasuga, M. Hiramatsu, A. Hoson, T. Sekino, K. Niihara, Langmuir 14 (1998) 3160-3163.
[21] Q. Chen, W.Z. Zhou, G.H. Du, L.M. Peng, Adv. Mater. 14 (2002) 1208.
[22] M.S. Sander, M.J. Cote, W. Gu, B.M. Kile, C.P. Tripp, Adv. Mater. 16 (2004) 2052.
[23] S. Lee, C. Jeon, Y. Park, Chem. Mater. 16 (2004) 4292-4295.
[24] S.M. Liu, L.M. Gan, L.H. Liu, W.D. Zhang, H.C. Zeng, Chem. Mater. 14 (2002) 1391-1397.
[25] R. Yoshida, Y. Suzuki, S. Yoshikawa, J. Solid State Chem. 178 (2005) 2179-2185.
[26] Y. Lan, X.P. Gao, H.Y. Zhu, Z.F. Zheng, T.Y. Yan, F. Wu, S.P. Ringer, D.Y. Song, Adv. Funct. Mater. 15 (2005) 1310-1318.
[27] D.Y. Zhang, L.M. Qi, Chem. Commun. (2005) 2735-2737.
[28] S.Z. Chu, S. Inoue, K. Wada, D. Li, H. Haneda, S. Awatsu, J. Phys. Chem. B 107 (2003) 6586-6589.
[29] S.Z. Chu, S. Inoue, K. Wada, D. Li, H. Haneda, J. Mater. Chem. 13 (2003) 866-870.
[30] J.G. Yu, H.G. Yu, B. Cheng, C. Trapalis, J. Mol. Catal. A 249 (2006) 135-142.
[31] H.Y. Zhu, X.P. Gao, Y. Lan, D.Y. Song, Y.X. Xi, J.C. Zhao, J. Am. Chem. Soc. 126 (2004) 8380-8381.
[32] H.Y. Zhu, Y. Lan, X.P. Gao, S.P. Ringer, Z.F. Zheng, D.Y. Song, J.C. Zhao, J. Am. Chem. Soc. 127 (2005) 6730-6736.
[33] S. Pavasupree, Y. Suzuki, S. Yoshikawa, R. Kawahata, J. Solid State Chem. 178 (2005) 3110-3116.
[34] H.G. Yu, J.G. Yu, B. Cheng, J. Lin, J. Hazard. Mater. 147 (2007) 581-587.

[35] H. Yu, J. Yu, B. Cheng, 253 (2006) 99-106.
[36] E.P. Barrett, L.G. Joyner, P.P. Halenda, J. Am. Chem.Soc. 73 (2002) 373-380.
[37] Y. Mao, M. Kanungo, T. Hemraj-Benny, S.S. Wong, J. Phys. Chem. B 110 (2005) 702-710.
[38] R. Ma, K. Fukuda, T. Sasaki, M. Osada, Y. Bando, J. Phys. Chem. B 109 (2005) 6210-6214.
[39] G. Busca, G. Ramis, J.M.G. Amores, V.S. Escribano, P. Piaggio, J. Chem. Soc. Faraday Trans. 90 (1994) 3181-3190.
[40] W.F. Zhang, Y.L. He, M.S. Zhang, Z. Yin, Q. Chen, 33 (2000) 912-916.
[41] K.R. Zhu, M.S. Zhang, Q. Chen, Z. Yin, 340 (2005) 220-227.
[42] A.R. Armstrong, G. Armstrong, J. Canales, P.G. Bruce, Angew. Chem. Int. Ed. 43 (2004) 2286-2288.
[43] T. Lopez, R. Gomez, E. Sanchez, F. Tzompantzi, L. Vera, 22 (2001) 99-107.
[44] M.A. Debeila, M.C. Raphulu, E. Mokoena, M. Avalos, V. Petranovskii, N.J. Coville, M.S. Scurrell, 396 (2005) 70-76.
[45] K.S.W. Sing, D.H. Everett, R.A.W. Haul, L. Moscou, R.A. Pierotti, J. Rouquerol, T. Siemieniewska, Pure Appl. Chem. 57 (1985) 603-619.
[46] D.V. Bavykin, V.N. Parmon, A.A. Lapkin, F.C. Walsh, J. Mater. Chem. 14 (2004) 3370-3377.
[47] R.I. Bickley, T. Gonzalez-Carreno, J.S. Lees, L. Palmisano, R.J.D. Tilley, J. Solid State Chem. 92 (1991) 178-190.
[48] D. Yang, H. Liu, Z. Zheng, Y. Yuan, J. Zhao, E.R. Waclawik, X. Ke, H. Zhu, J. Am. Chem. Soc. 131 (2009) 17885-17893.
[49] M.A. Fox, M.T. Dulay, Chem. Rev. 93 (1993) 341-357.

List of Figures

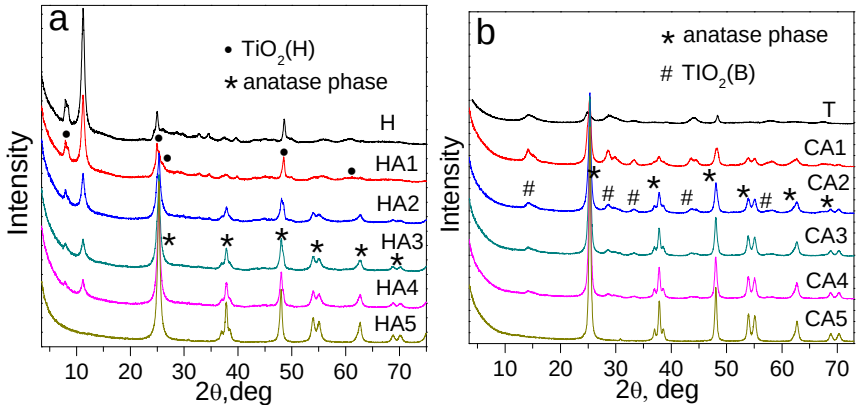

Fig. 1.

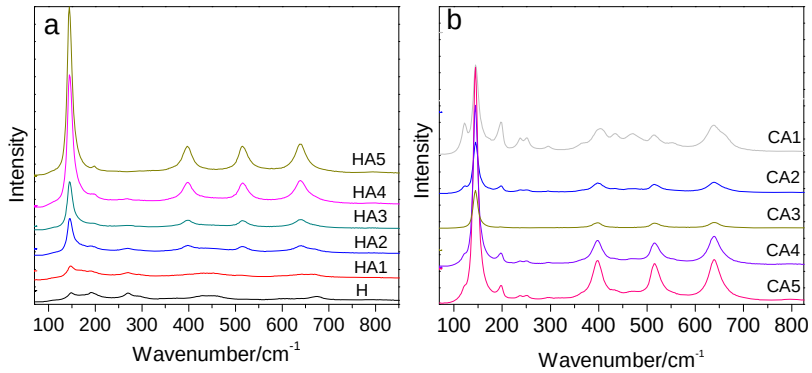

Fig. 2.

Comment [M1]: ????

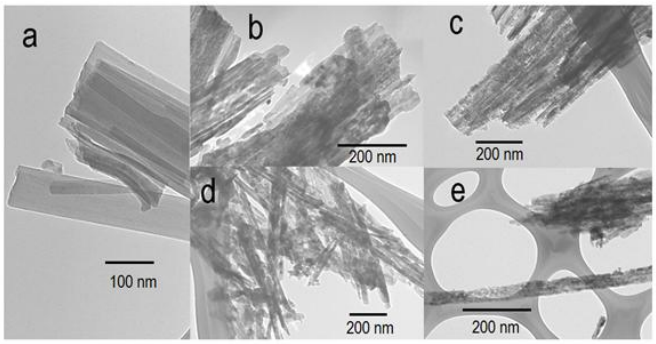
a
b
c
d
e
100 nm
200 nm
200 nm
200 nm
200 nm

Fig. 3.

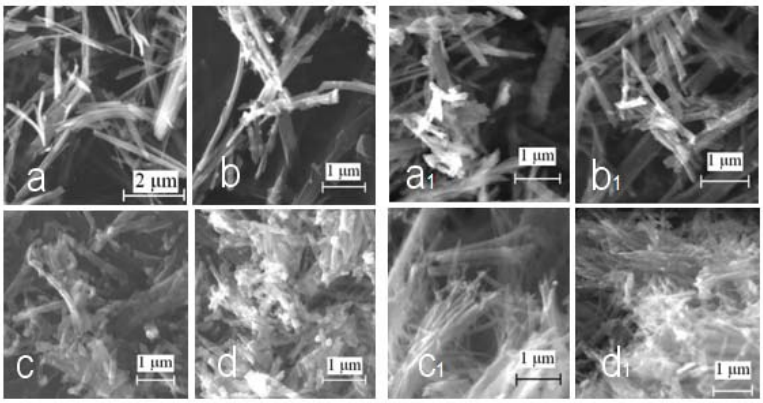
a
2 μm
b
1 μm
a1
1 μm
b1
1 μm
c
1 μm
d
1 μm
c1
1 μm
d1
1 μm

Fig. 4.

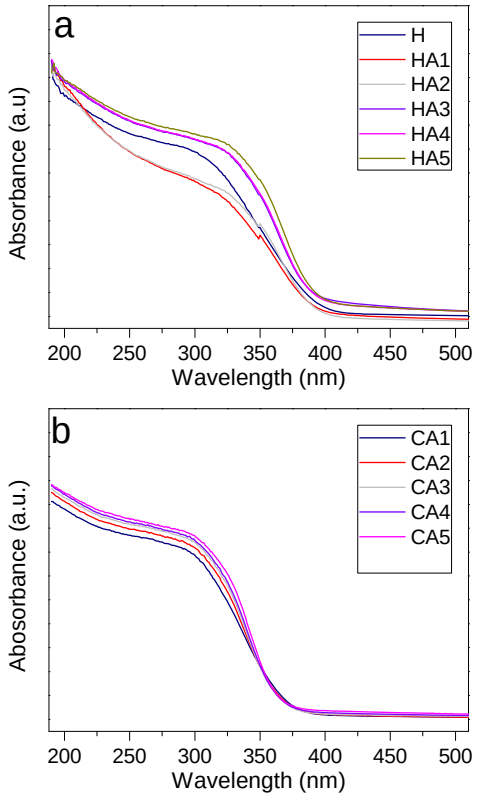
a
H
HA1
HA2
HA3
HA4
HA5
Absorbance (a.u)
200 250 300 350 400 450 500
Wavelength (nm)
b
CA1
CA2
CA3
CA4
CA5
Abosorbance (a.u.)
200 250 300 350 400 450 500
Wavelength (nm)

Fig. 5.

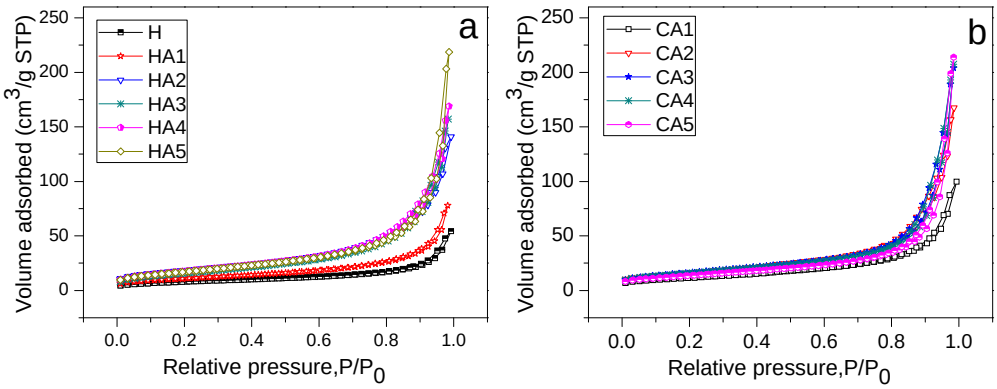
a
H
HA1
HA2
HA3
HA4
HA5
Volume adsorbed (cm3/g STP)
0 50 100 150 200 250
0.0 0.2 0.4 0.6 0.8 1.0
Relative pressure,P/P0
b
CA1
CA2
CA3
CA4
CA5
Volume adsorbed (cm3/g STP)
0 50 100 150 200 250
0.0 0.2 0.4 0.6 0.8 1.0
Relative pressure,P/P0

Fig. 6.

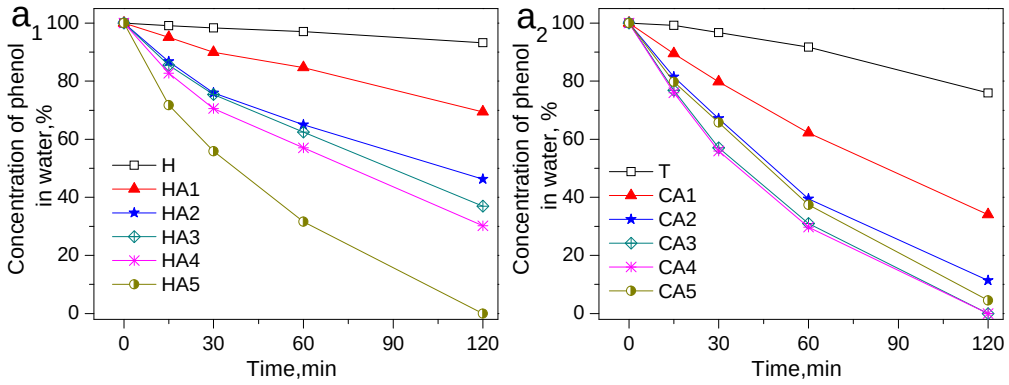
a1
Concentration of phenol in water,%
Time,min
H
HA1
HA2
HA3
HA4
HA5
a2
Concentration of phenol in water, %
Time,min
T
CA1
CA2
CA3
CA4
CA5

Fig. 7.

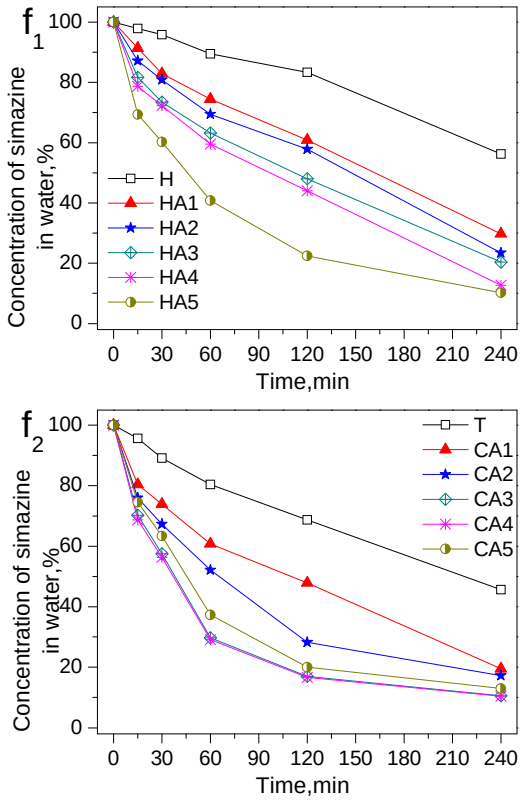
f1
Concentration of simazine in water,%
Time,min
H
HA1
HA2
HA3
HA4
HA5
f2
Concentration of simazine in water,%
Time,min
T
CA1
CA2
CA3
CA4
CA5

Fig. 8.

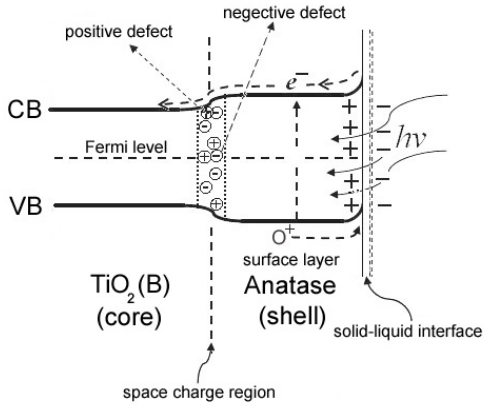
negective defect
positive defect
e⁻
CB
Fermi level
VB
hν
O⁺
surface layer
TiO2(B)
(core)
Anatase
(shell)
solid-liquid interface
space charge region

Fig. 9.

List of Tables

Table 1

Effects of hydrothermal treatment and calcination on the BET specific surface area (S_{BET}) and crystal size of mixed phase fibres.

Samples	S_{BET} ($m^2.g^{-1}$)	V_p[a] ($cm^3.g^{-1}$)	Mean D (nm) BET[b]	Mean D (nm) BJH[c]	D_A (nm)
H	28.4	0.08	11.8	12.4	0
HA1	39.4	0.12	12.2	12.0	10.16
HA2	66.5	0.22	13.1	12.0	11.73
HA3	57.3	0.24	17	13.9	12.35
HA4	64	0.26	16.4	13.9	13.46
HA5	62	0.33	22	18.1	16.15
CA1	42.1	0.15	14.6	13.2	11.1
CA2	58	0.26	18	15	12.9
CA3	59	0.31	21.4	18	14.98
CA4	57	0.32	22.6	19	16.99
CA5	49	0.33	27	22	17.9

[a] Single point adsorption total pore volume of pores at P/P_0 0.99. [b] Adsorption average pore diameter(4V/A by BET). [c] Barrett–Joyner–Halenda(BJH) desorption average pore diameter(4V/A).